Impact of protein aggregation on the immunogenicity of a human monoclonal antibody following pulmonary administration in mice

Sohaib Mahri[1], Céline Cassiers[1], Sandra Gracin[2], Donatienne Tyteca[3], Francine Uwambayinema[4], François Huaux[4], Mariam Ibrahim[5], Sian Piper[6], Antonio Llinas[2], Markus Fridén[2], Rita Vanbever[1, *]

[1] Université catholique de Louvain (UCLouvain), Louvain Drug Research Institute (LDRI), Advanced Drug Delivery & Biomaterials (ADBB), Brussels 1200, Belgium.

[2] AstraZeneca; Pharmaceutical Technology & Development; Inhalation Product Development; Gothenburg, Sweden

[3] UCLouvain, de Duve Institute, CELL Unit and PICT Imaging Platform, Brussels, Belgium

[4] UCLouvain, Institut de Recherche Expérimentale et Clinique, Louvain Centre for Toxicology and Applied Pharmacology, Brussels, Belgium

[5] AstraZeneca; R&D Biopharmaceuticals; Biopharmaceuticals Development; Gaithersburg, US

[6] AstraZeneca; R&D Biopharmaceuticals; Bioscience Asthma and skin Immunity, Early R&I; Cambridge, UK

*Corresponding author at: Université catholique de Louvain, Louvain Drug Research Institute, Advanced Drug Delivery and Biomaterials, Avenue Emmanuel Mounier 73, Brussels 1200, Belgium. Tel.: +32 2 764 73 25; fax: +32 2 764 73 98. E-mail address: rita.vanbever@uclouvain.be.

Abbreviations

ADA, anti-drug antibody; AM, alveolar macrophage; BAL, bronchoalveolar lavage fluid; DC, dendritic cell; DLS, dynamic light scattering; DOL, degree of labelling; FBS, Foetal Bovine Serum; Hi_Agg_DP, dry powder of rhod-NIP228 with high level of aggregates; IM, interstitial macrophage; IT, Intratracheal; Lo_Agg_DP, dry powder of rhod-NIP228 with low level of

aggregates; MFI, median fluorescence intensity; MW, molecular weight; No_Agg_Sol, Aggregate-free rhod-NIP228; OD, optical density; PBS, phosphate buffer saline; PS80, polysorbate 80, RSD, relative standard deviation; SC, subcutaneous injection; SEC, size exclusion chromatography; SEM, standard error of the mean.

1. Abstract

Spray drying is a widely employed method for generating dry powder formulations for inhalation. Yet, it presents substantial challenges when applied to therapeutic proteins due to stability issues. The formation of protein aggregates during the atomization and the heating steps can diminish protein activity and raise immunogenicity concerns. Here, we assessed the impact of varying levels of protein aggregates generated during spray-drying on the fate and the immunogenicity of the human monoclonal antibody NIP228 following intratracheal administration in mice. Aggregate-free rhodamine labelled NIP228 was spray-dried with or without 1% polysorbate 80 surfactant, resulting in the generation of powder formulations with associated low and high protein aggregate levels, respectively. Confocal imaging highlighted the presence of aggregates in the lungs for both powders but not for the solution, while flow cytometry analysis designated alveolar macrophages as the main immune cells taking up rhod-NIP228 in the lungs with very little involvement of dendritic cells and interstitial macrophages following a single dose administration. Notably, repeated intratracheal administration of the three formulations in mice did not impact the magnitude of the anti-drug antibody response in sera or broncho-alveolar lavages. The pulmonary route appeared to evoke a more robust immune response when compared to subcutaneous administration. Overall, the level of NIP228 aggregation in this study did not appear to be the primary driver of NIP228 immunogenicity following delivery to the lungs in mice, shedding new light on the interplay between protein aggregation and immunogenicity in the context of the pulmonary delivery of therapeutic proteins.

Keywords: Anti-drug antibody (ADA), immunogenicity, pulmonary delivery, monoclonal antibody, spray drying.

2. Introduction

Accelerated growth of biopharmaceuticals has transformed the landscape of the healthcare and pharmaceutical industry in recent years (Walsh, 2018). Therapeutic proteins, the predominant category of biopharmaceuticals in the market, are typically administered through the parenteral route in lung diseases (Desoubeaux et al., 2016). Nevertheless, systemic administration results in a low drug fraction in the lung tissue compared to blood and other tissues. Consequently, higher doses of the protein are required for treating respiratory diseases, leading to increased costs in protein manufacturing as well as the risk of systemic side effects. Local delivery by inhalation, on the other hand, promotes a rapid onset of action and a higher lung availability at lower doses, thus limiting toxicity concerns related to systemic administration (Labiris and Dolovich, 2003; Osman et al., 2018). The appeal of local delivery by inhalation is therefore strong for the treatment of respiratory diseases such as asthma, cystic fibrosis (CF), chronic obstructive pulmonary disease (COPD), lung cancer, and respiratory infections. Yet, only two inhaled biologics have been approved in the last three decades (rhDNase, Pulmozyme®, and insulin, first as Exubera® [now withdrawn from the market], then Afrezza®). The success rate for inhaled biologics falls short when compared to other routes of administration. Although several inhaled biologics are under development, no other biologics have reached the market so far, underscoring the significant challenges in developing biologics through this route of administration (Ibrahim et al., 2023).

Proteins intended for inhalation can be formulated as solutions or dry powders. Compared to liquid formulations, the solid state provides improved protein stability and convenient delivery using dry powder inhalers. A cost-effective, reproducible, and scalable method of producing inhalation dry powders is through spray drying (Chang et al., 2021; Eedara et al., 2021). This process allows the generation of readily dispersible powders with appropriate aerodynamic properties. Although spray drying is a well-established process for small molecules, the steps of atomization and heating inflict physical stresses on proteins, which may cause protein unfolding and aggregation and lead to a potential loss of bioactivity and an increased risk of immunogenicity (Rosenberg, 2006; Tao et al., 2023). Production of anti-drug antibodies (ADAs), a typical immune response to protein therapeutics, can lead to complications ranging from minor alterations of pharmacokinetics to reduced efficacy and severe adverse reactions

(e.g., anaphylaxis) causing treatment discontinuation (Shankar et al., 2015). The occurrence of ADAs, both neutralizing and not, should therefore be investigated. Their impact on pharmacokinetics and efficacy should be carefully assessed to provide adequate safety data to regulatory agencies (FDA, 2014; Hall et al., 2021).

Abundant literature is available on the correlation between aggregates and immunogenicity of therapeutic proteins delivered by the parenteral route (Jiskoot et al., 2016). Protein aggregates are thought more immunogenic than soluble protein monomers because protein aggregates are readily taken up by antigen-presenting cells. Despite this, similar studies by the pulmonary route are scarce while the inhalation route of administration is associated with increased immunogenicity (FDA, 2014; Hall et al., 2021). Only one recent article reports on the delivery of protein aggregates to the lungs and its immunological consequences: aggregates of a murine IgG were generated by nebulization and the protein aggregates were shown to activate immune cells in vitro and to deplete immune cells in the lungs following intratracheal instillation in mice (Secher et al., 2022).

In an effort to gain more insights into the immunogenicity of proteins by the inhalation route and whether it is influenced by protein aggregates caused by the spray drying process, we investigated the impact of different levels of protein aggregates on the immunogenicity of the human monoclonal antibody (mAb) NIP228 following repeated intratracheal administration (IT) in mice. NIP228 is a human mAb raised against 4-hydroxy-3-iodo-5-nitrophenylacetic acid. NIP228 was used as a model protein in this study as it does not recognise any target in mice. To examine the fate of NIP228 in the lungs, the antibody was labeled with NHS-rhodamine and the aggregate-free solution of rhod-NIP228 (No_Agg_Sol) was spray-dried with and without PS80 surfactant (PS80) in the dry powder (1% w/w) to generate low and high levels of NIP228 aggregates (Lo_Agg_DP and Hi_Agg_DP, respectively). Both powders were made of 10% w/w rhod-NIP228 and 90% w/w excipients including trehalose, trileucine and histidine. The fate of the three rhod-NIP228 formulations in the lungs was examined by confocal microscopy and the uptake of rhod-NIP228 by alveolar macrophages and antigen-presenting cells was assessed by flow cytometry following intratracheal administration.

3. Material and Methods

3.1. Materials

The mAb NIP228 was obtained from AstraZeneca (Cambridge, UK), NHS-rhodamine was purchased from Life Technologies (Gent, Belgium). SulfoCyanine5 and NHS-AlexaFluor568 were purchased from Lumiprobe (Gentaur Europe, Kampenhout, Belgium). PS80 (or tween® 80) was purchased from Sigma-Aldrich (St. Louis, MO, USA; purity ≥99). Unless otherwise mentioned, all other chemicals and reagents were purchased from Sigma-Aldrich (St. Louis, MO, USA). Crystalline D-(+)-trehalose dihydrate was bought from Hayashibara Co (Japan; purity ≥99), and raw crystalline trileucine was bought from Bachem, UK (Cat. No. H-3915; purity ≥98).

3.2. NIP228 fluorescent labelling

The most suitable fluorescent dye to label NIP228 was first selected. The dye needed to be as small and hydrophilic as possible to limit the alteration of NIP228 physicochemical properties. It also needed to present a high brightness and an excitation wavelength in the red channel to limit the tissue autofluorescence. On these bases, three dyes, Rhodamine, SulfoCyanine5 and AlexaFluor568, were pre-selected (Table S1). We then assessed the lung tissue binding property of the three dyes and we further excluded AlexaFluor568 as it mainly partitioned in the lung homogenate compartment with a ratio of dialysate to lung homogenate compartment concentrations of 20%, against 89% and 102% for Rhodamine and SulfoCyanine5, respectively (Table S2).

Next, NIP228 labelling assays were performed with NHS-rhodamine and NHS-SulfoCyanine5. NIP228 solution was received at a concentration of 9.69 mg/ml in a storage solution of 50 mM trehalose and 20 mM histidine (purity ≥99). To avoid the undesirable reaction of the NHS functional group with the amine group of histidine, NIP228 stock solution was exchanged against phosphate buffer saline (PBS, pH 7.45, Gibco™, Life Technologies, Gent, Belgium) by dialysis (Spectra/Por molecular porous membrane tubing MWCO 6–8 kD, Spectrum). NHS-rhodamine or NHS-SulfoCyanine5 (10 mg/ml in DMSO) was added to NIP228 solution at a molar ratio of 2:1, was mixed by pipetting and left to react for 2 hours at 4 °C in the dark. The excess of unreacted dye was removed by dialysis against a solution of PBS and then 3 times

against the 50 mM trehalose and 20 mM histidine solution. The final solution of labelled NIP228 was centrifuged at 10,000g for 10 min, and the supernatant was stored at -20 °C until spray drying. A degree of labelling (DOL, molecules of dye per molecule of NIP228) of 1.2 and 2.6 was achieved for rhodamine-NIP228 (rhod-NIP228) and SulfoCyanine5-NIP228, respectively. The reaction yield was high with NHS-rhodamine but low with NHS-SulfoCyanine5 with respectively 75% and 37% recovery of the NIP228 quantity involved. We noticed that SulfoCyanine5-NIP228 precipitated on the membrane during dialysis, which might explain the low reaction yield (Fig S1). NHS-rhodamine was finally selected as the most suitable dye to label NIP228 as SulfoCyanine5 largely destabilized NIP228 when exposed to an air liquid interface while rhodamine did not alter NIP228 stability (Fig S2).

3.3. Spray drying

Two dry powders were prepared in this study, with and without the addition of PS80 (Lo_Agg_DP and Hi_Agg_DP, respectively). The feed solutions were prepared using MilliQ water with a total solid content of 30 mg/ml: rhod-NIP228 (10 % w/w), trehalose (81% w/w), trileucine (5% w/w), histidine (4% w/w). Spray-dried amorphous trileucine was used to prepare NIP228 solutions to avoid issues with low solubility. Raw crystalline trileucine was used in the preparation of the amorphous batch. The spray drying process was designed to yield a physically stable and inhalable amorphous powder. A modified Büchi B-290 spray dryer (Büchi Labortechnik AG, Switzerland) equipped with Büchi twin fluid atomizer and nitrogen atomizing gas was used (0.7 mm liquid nozzle and 1.5 mm gas cap orifice diameter). Spray drying parameters were as follow: inlet and outlet temperatures of 95 °C 54°C, respectively; 2 ml/min feed flow rate; 1850 l/h atomizing gas flow rate; 100% aspiration rate (corresponding to 23.5 kg/h drying gas flow rate). The dry powder was removed from the collection vessel in a humidity-controlled laboratory at 6% relative humidity (RH) and stored in a closed container at 2% RH cabinet. Within a week from manufacturing, dry powders were filled in capsules (ca. 10 mg powder) same conditions and packaged in individual hermetically sealed pouches.

3.4. Characterization of rhod-NIP228 formulations

- **Dynamic light scattering (DLS)**

The hydrodynamic size of rhod-NIP228 in different formulations was measured using DynaPro II/III Plate Reader DLS instrument from Wyatt Technologies (Santa Barbara, CA, USA). Data were recorded and analyzed using built-in DYNAMICS software assuming a globular protein model. Powders were reconstituted in 20 ml plastic bottles using MilliQ water at a concentration of 2.6 mg/ml of rhod-NIP228. Bottles were then manually swirled and placed on a Stuart SRT6D roller mixer (Stuart Scientific, UK) at 60 RPM for 1 h before acquisitions. 100 µl of rhod-NIP228 solution or reconstituted dry powders (Hi_Agg_DP and Lo_Agg_DP) were placed in 96 well plates, and 10 runs were acquired for each well at room temperature using 826 nm laser wavelength.

- **Size exclusion chromatography (SEC)**

The three formulations (No_Agg_Sol, Hi_Agg_DP, and Lo_Agg_DP) were analyzed by SEC. Solution or reconstituted dry powders in water were centrifuged at 10,000 g for 10 min to eliminate insoluble aggregates. The supernatant was injected in Superdex 75 Increase 10/300 GL column (Cytiva, Belgium) on ÄKTA™ purifier 10 system (GE Healthcare Bio-Sciences AB, Uppsala, Sweden). Samples were eluted by PBS pH 7.45, and peaks were monitored at 280 nm (protein) and 555 nm (labelling dye).

- **Confocal microscopy**

Three µl of rhod-NIP228 solution or reconstituted powders (2 mg/ml rhod-NIP228) were placed on cover glass (thickness No. 1 # 631-0146, VWR International BVBA, Leuven, Belgium) and examined immediately by Cell Observer Spinning Disk (COSD, Zeiss, Germany). Images were recorded (25x) using 561 nm (rhod-NIP228) and 405 nm (tissue autofluorescence) laser lines. Images were processed using ImageJ software (1.47v, NIH, USA).

- **Gel electrophoresis**

NIP228 or rhod-NIP228 (from solution or reconstituted dry powders) was diluted in PBS then 2-4 µg protein was mixed with the loading buffer (Native Sample Buffer for Protein Gels, BioRad, Belgium) and loaded onto SDS-PAGE gel (4–20% Mini-PROTEAN® TGX™ Precast Protein Gels, BioRad, Belgium). The gels were run at 120-150 V for 60-80 min in

Tris/Glycine/SDS electrophoresis buffer (BioRad, Belgium) then stained using coomassie blue staining (GelCode™ Blue Stain Reagent, Thermofisher, Gent, Belgium).

- **Microflow imaging**

The microflow imaging 5200 series system with a 100-µm flow volume and microflow imaging View system software, version 5.1.076 S/N 1999 (Protein Simple, San Jose, CA) was used for quantification of subvisible particles (size < 100 µm) post powder reconstitution. An aspect ratio filter of 0.85 was applied to exclude particles with an aspect ratio of >0.85, thereby allowing air bubbles to be excluded as needed. Particle diameter was reported as equivalent circular diameter (ECD). Rhod-NIP228 dry powders (Hi_Agg_DP and Lo_Agg_DP) were reconstituted in water for injection at a protein concentration of 5 mg/ml.

- **Particle size, density and morphology**

The primary geometric particle diameter (d) of the dry powders was measured by laser diffraction (HELOS, Sympatec, Clausthal-Zellerfelg, Germany). Powder samples were suspended in cyclohexane in a 50 ml glass cuvette and stirred with a magnetic bar at 1000 rpm. A short period of sonication (30 to 60 s) at a power of 60 W (CUVETTE, Sympatec; 8.5 mm diameter ultrasound tip) was applied before sizing. A R2 lens allowing measurements in the range of 0.25–87.5 µm was used. The particle size analysis was performed by the WINDOX 3.4 software, and the mass median particle diameter (D50) was taken into account.

The powder density (ρ) was determined by tap density measurements, i.e., following 1000 taps which allowed the density to plateau. The particle density which is involved in the notion of aerodynamic diameter is the "sphere-envelope" mass density, i.e., the density of the particles with internal pores. Tap density measurements well estimate the "sphere-envelope" mass density (Vanbever et al., 1999).

The primary aerodynamic diameter of the particles, daer, was calculated based on the following definition (valid for spherical particles): $daer = d \times \sqrt{\rho/\rho 1}$ with ρ_1 = 1 g/cm^3 (Vanbever et al., 1999).

The particle morphology was examined by using a Zeiss GeminiSEM 300 scanning electron microscope (Carl Zeiss Microscopy GmbH). The spray-dried powders were mounted onto a carbon plate and imaged using a second electron detector at 1.0kV in high vacuum mode.

- **Aerosol characterisation**

The aerosol properties of the powders were characterized using a Next Generation Impactor (NGI, Copley Scientific, UK) fitted with the RS01 single dose capsule device (Plastitape, Italy), applying a 4 kPa pressure drop corresponding to a flow rate of 60 L/min. The RS01 device was used as a means to aerosolize the powder from the capsule. The selected pressure-drop (and flow rate) is a consistent compendial quality testing, representing patient inhalation flow using common dry powder inhalers. The Fine Particle Dose (FPD), the Mass Median Aerodynamic Diameter (MMAD) and the Geometric Standard Deviation (GSD) were calculated as instructed by the European Pharmacopoeia v9.0 (Council-of-Europe, 2017. European Pharmacopoeia, 9.0 ed. European directorate for the quality of medicines & healthcare). The Fine Particle Fraction (FPF) was expressed as a percentage of the FPD to the device dose. Due to technical challenges, there was no NGI-based aerosol characterization done to mimic in vivo delivery in mice.

3.5. Fate of rhod-NIP228 in the lungs by confocal microscopy

3.5.1. Mice

Female RjOrl SWISS mice (Elevage Janvier, Le Genest-St-Isle, France) were used for all experiments. Mice were received at 6 weeks of age and were allowed to acclimate for at least one week before experiments. They were fed a normal chow diet and had water ad libitum. Anaesthesia was induced by intraperitoneal injection of a solution of ketamine/xylazine (90/10 mg/kg) and was confirmed by the absence of pedal reflex following firm toe pinch. All animal experiments were approved by the Institutional Animal Care and Use Committee of the Université catholique de Louvain (Permit number 2019/UCL/MD/044).

3.5.2. In vivo delivery of rhod-NIP228

Throughout all experiments, a dose of 50 µg of rhod-NIP228 (0.33 nmol) was given to mice by intratracheal instillation or subcutaneous injection (SC, solution) or by intratracheal

insufflation (Hi_Agg_DP and Lo_Agg_DP powders). Aliquots of frozen solution of rhod-NIP228 (-20 °C) were thawed then centrifuged at 10,000 g for 10 min before use. NIP228 is stable frozen and NIP228 and rhod-NIP228 endured at least three cycles of freeze-thawing.

- **Intratracheal instillation**

Anesthetized mice were held in a supine position on an inclined board (~ 30°) then were intubated with a 20G catheter (VWR International bvba, Leuven, Belgium) with the help of a Penn-Century™ laryngoscope (Model LS-2 for small rodents, Philadelphia, USA). 50 µg of rhod-NIP228 solution (50 µg/25 µl) were instilled intratracheally directly into the lungs using a Hamilton precision syringe (Model 710, Bonaduz, Switzerland). Instillation was immediately followed by an air bolus of 200 µl (1 ml HSW Soft-Ject™, VWR International bvba, Leuven, Belgium).

- **Intratracheal insufflation**

The equivalent of 50 µg of rhod-NIP228 (~ 0.55 mg powder at ~ 9% drug loading) were insufflated into mice trachea using the Penn-Century insufflator (Model DP-3, Penn-Century, Inc., Philadelphia, PA, USA). The insufflation method was adapted from the work of Morello *et al.* in which a polyethylene (PE) tubing was used to load the accurate weight of powder [17]. PE tubing with an inner diameter of 0.8 mm and outer diameter of 0.97 mm (PE50, BD Intramedic™, Fisher Scientific, Belgium) was cut into 2.6 cm long pieces. The powder was then loaded by dipping one end of the PE tubing into the dry powder (Fig S3 a) until the appropriate weight was attained. The loaded PE tubing was loaded into the insufflator chamber then the insufflator was assembled and attached to 1 ml syringe (200 µl of air) (Fig S3 b-d). The accuracy of the delivery system was established in a pilot study and was around ± 13% of the loaded dose (Fig S3 e).

Mice were intubated with a 20G catheter as described above, and then the insufflator delivery tube was inserted into the trachea of intubated mice through the catheter. The powder was then released by firmly thrusting the syringe plunger to deliver 200-250 µl air puffs. In the majority of cases, one air puff was enough to deliver the entire loaded dose; however, extra puffs were administered if necessary. The exact delivered dose was deduced by weighing the insufflator before and after insufflation. After each insufflation, the insufflator was dismantled

and inspected to make sure the whole dose was delivered then flushed with a high flow rate of N_2 to clean it.

Dry powder handling and animal insufflations were performed in a room with controlled relative humidity (RH) of 25-35 %. Individual dry powder capsules were kept in sealed pouches and used within 40 min of opening to avoid any alteration of the powder due to the humidity.

- **Subcutaneous injection**

Mice were subcutaneously injected with 100 µl of 0.5 mg/ml rhod-NIP228 solution (50 µg of rhod-NIP228) on the right flank using 0.5 ml insulin syringes (BD Micro-Fine™, VWR International BVBA, Leuven, Belgium).

3.5.3. Confocal imaging

Mice received 50 µg of rhod-NIP228 by instillation (in 25 µl solution) or insufflation (~ 0.55 mg dry powder) as described in the previous section (3.5.2). At times 0h, 4h, and 16h post-delivery mice were euthanized by cervical dislocation then bled by cutting the vena cava. Whole lungs were removed, rinsed in saline, then immediately sectioned by a razor blade while still fresh (Fig S4 a-b). Sections were placed on a cover glass and examined without staining by laser scanning confocal microscopy (Cell Observer Spinning Disk, Zeiss, Germany). Two mice were used per group and time point. Based on our experience, immersing fresh lung sections in a 4% formaldehyde PBS solution to fix the lung tissue resulted in the formation of artefactual protein aggregates and the alteration or loss of the tested compound's local distribution.

The blue (405 nm, 1000ms, autofluorescence) and yellow (561 nm, 200ms, rhod-NIP228) channels were used to capture images (Fig S4 c-e) at a magnification of 25. All images were saved in 16-bit format and processed using ImageJ software (1.47v, NIH, USA). Unspecific autofluorescence background was eliminated by selecting a cut-off threshold for the detection rhod-NIP228 (Fig S4 c&f).

3.6. Immunogenicity of rhod-NIP228 for different formulations and administration routes

Mice (n = 10) received 5 weekly administrations of 50 µg of rhod-NIP228 by intratracheal instillation (25 µl solution), intratracheal insufflation (~ 0.55 mg dry powder) or SC injection (100 µl solution). The control group received a saline solution by intratracheal instillation (n =

4). Blood was collected by tail snipping at day 20, one day before the fourth dose. On day 46, 18 days after the last dose, mice were euthanized by cervical dislocation and blood and bronchoalveolar lavage fluid (BAL) were collected. Blood was allowed to clot at +4°C for 24h then sera were collected after centrifugation at 500 g for 15 min. BAL was collected using 2 × 1 ml Hank's Balanced Salt Solution (HBSS, no Ca^{+2}, no Mg^{+2}, Gibco™, Life Technologies, Gent, Belgium), centrifuged at 500 g for 10 min and the cell-free supernatant was kept. Sera and BAL were stored at -20°C for anti-drug antibodies (ADAs) quantification.

Levels of anti-drug (anti-NIP228) antibodies (ADAs) were measured in sera and BAL by an in-house enzyme-linked immunosorbent assay (ELISA). 96-well plates (Nunc-Immuno Plate Maxisorp, Surface, Gibco BRL Life Technologies, Gent, Belgium) were coated with NIP228 (4 µg/mL) in 1% $NaHCO_3$ solution, pH 9.6, and incubated at 4°C overnight. The next day, plates were washed with PBST (0.05% (v/v) Tween 20 in PBS) then blocked with 1% BSA in PBST for 1h at room temperature (RT). Serial dilutions of sera or BAL were made in 1% BSA in PBST and plates were incubated for 2h at room temperature, then detection antibody was added for 1h at RT (Goat anti-mouse/rat*HRP 1/5000, Becton Dickinson Benelux). A colorimetric substrate of HRP was then added (1-Step™ Ultra TMB-ELISA Substrate Solution, Thermofisher, Gent, Belgium) and plates were watched until a blue coloration had developed (~ 2 min). The reaction was stopped by adding 2 M H_2SO_4. Absorbance values were recorded by SpectraMax iD5 microplate reader (Molecular Devices, CA, USA). Optical densities ODs (OD 450 nm – OD 540 nm) were plotted against the dilution factor, and data were fitted using Four Parameter Logistic (4PL) Regression (Fig S5 a & c). The titer was defined as the reciprocal of the dilution that gives an OD (450 nm – 540 nm) equal to a predefined cut-off (0.1 for sera and 0.03 for BALs). A titer of zero (0) was arbitrarily attributed to samples of serum and BAL where the undiluted samples gave ODs below the predefined cut-offs. For simplicity, the corresponding *log* titers (of samples of titer zero) were also plotted as zero (0) on the y-axis. Note that titers in the serum and BAL samples are not comparable as different cut-offs were used for sera and BALs (0.1 and 0.03, respectively). An internal control (randomly chosen serum from Hi_Agg_DP group) was included in each plate to account for inter-plate variations (Fig S5 b and d). All sera or BAL samples were analyzed the same day in the same conditions.

3.7. Uptake of rhod-NIP228 by lung cells in vivo

Uptake by alveolar macrophages (AMs), lung dendritic cells (DCs), and lung interstitial macrophages (IMs) was assessed 16h post-administration of 50 µg of rhod-NIP228 to Swiss mice (n =5). Control mice did not receive any formulation. 16 h post-delivery mice were euthanized by cervical dislocation and mice were exsanguinated by cutting the vena cava, then BALs were immediately collected using 2 x 1ml HBSS through the cannulated trachea. BALs were centrifuged at 500 g for 10 min and the cell pellets were re-suspended in ACK to lyse red blood cells, then centrifuged again to collect cells in PBA (PBS with 1% albumin) for further staining and flow cytometry. Lungs were perfused until they became pale through the pulmonary artery by inserting 26G needle into the heart right ventricle and injecting several millilitres of saline. Lungs were then infused through the trachea with 1 ml of pre-warmed (37 °C) digestion solution containing 2 mg/ml pronase and 0.1 mg/ml DNase (Worthington Biochemical, Lakewood, NJ, USA) with 1% antibiotic antimycotic and fungizone (25 mg/mL; Life Technologies, Gent, Belgium). After 20 min, the enzymatic reaction was stopped by removing the lungs and placing them in 2 ml Foetal Bovine Serum (FBS) to be mechanically dispersed with a 20 mL syringe, then filtered through a 70 µm cell strainer (BD Biosciences, Bedford, MA, USA).

Flow cytometry was used to discriminate AMs, IMs, and DCs in lung cell suspensions and BAL as described in (Vanbever et al., 2019). AMs were identified as $CD45^{hi}$ $F4/80^{hi}$ $CD64^{hi}$ $CD11c^{hi}$ Siglec-F^{hi} $CD11b^{lo}$ cells; IMs as $CD45^{hi}$ $F4/80^{hi}$ $CD64^{hi}$ $CD11c^{hi}$ $CD11b^{hi}$ Siglec-F^{lo} cells; DCs as $CD45^{hi}$ $CD64^{lo}$ $CD11c^{hi}$ $MHCII^{hi}$ cells. The gating strategy is shown in Fig S6. Fluorochrome-conjugated monoclonal antibodies specific to the mouse antigens were used: anti-CD45 (clone 30-F11, APC-Cy7; BD Biosciences, Oxford, UK), anti-F4/80 (clone BM8, APC; eBioscience, Vienna, Austria), anti-CD11c (clone HL3, PE-Cy7; BD Biosciences), anti-CD64 (clone X54-5/7.1, FITC; BD Biosciences), anti-Siglec-F (clone E50-2440, BV421, BD Biosciences), anti-CD11b (clone M1/70, BV421, BD Biosciences), and anti-MHCII/I-A/I-E (Clone 2G9, FITC; BD Biosciences). Dead cells were excluded from quantification using live and dead cell discriminator (LIVE/DEAD™ Fixable Lime (506), Thermofisher, Gent, Belgium). Samples were acquired on a BD LSR Fortessa (BD Biosciences) and analyzed using FlowJo software (TreeStar, Ashland, OR, USA).

3.8. Uptake of rhod-NIP228 by macrophages in vitro

Murine AMs MHS (ATCC® CRL-2019™) were cultured at 37 °C and 5% CO_2 in a complete cell culture medium of RPMI-1640 medium supplemented with 10% heat-inactivated FBS and 0.05 mM 2-mercaptoethanol. Cells were subcultured every 2–3 days and were used between passages 7 and 11.

10^5 cells/well (1 ml) were seeded in 24-well plates and incubated for 24 h. The next day, cells were exposed to 5 µg/ml of rhod-NIP228 in complete cell culture medium for 16h at 37 °C and 5% CO_2. Solution of rhod-NIP228 were directly diluted in complete cell culture medium whereas Hi_Agg_DP and Lo_Agg_DP dry powders were first reconstituted in water then diluted in complete cell culture medium. After incubation, cells were washed five times with PBS, detached by 0.25% trypsin-EDTA solution then centrifuged at 300 g for 5 min. Cell pellets were re-suspended in PBA for flow cytometry analysis (LSR Fortessa, BD Biosciences, San Jose, USA).

3.9. Statistics

ANOVA was used for multiple group comparisons ($n \geq 3$). For ADA titers, ANOVA was used for multiple group comparisons on log-transformed data. Unless otherwise mentioned, data are presented as mean ± sem. All statistical inferences are based on a two-sided significance level of * $p < 0.05$, ** $p < 0.01$, and *** $p < 0.001$ and were carried out using GraphPad Prism version 8.00 (GraphPad Software, La Jolla California USA). Optical densities vs dilution factor plots were fitted using Four Parameter Logistic (4PL) Regression (Fig S5).

4. Results

4.1. Spray drying of rhod-NIP228

NIP228 was first labeled with NHS-rhodamine then spray dried in the presence of trehalose (81% w/w), trileucine (5% w/w), and histidine (4% w/w). Rhod-NIP228 was incorporated at a final percentage of roughly 10% (w/w) of the final formulation in the presence or absence of 1% PS80. As the feedstock formulation and spray drying parameters influence the dry powder physical characteristics and aerodynamic properties, and ultimately the deposition within the respiratory tract, morphology, particle size distribution, tap density, and aerodynamic characteristics of the spray-dried powders with and without the addition of 1% PS80 were assessed (Fig 1).

Scanning electron microscope (SEM) showed wrinkled and corrugated particles of sizes from < 1 µm and up to about 5 µm and no discernible difference between Hi_Agg_DP (no PS80) and Lo_Agg_DP (1% PS80) (Fig 1a&b). Both powders appeared to be well dispersed and did not contain a significant number of particle agglomerates or particles above 5 µm in size. Laser diffraction confirmed a particle size (d) around 3 µm for both powders. The tap powder density (ρ) was 0.4 and 0.5 g/ml for the Hi_Agg_DP and Lo_Agg_DP, respectively (Fig. 1d).

The NGI data indicated a comparable in vitro deposition pattern for the Hi_Agg_DP and Lo_Agg_DP (Fig 1c), expect for the FPF < 5 µm which was higher for the Lo_Agg_DP (88.6 ± 0.3%) compared with the Hi_Agg_DP (78.3 ± 1.6 %) ($p = 0.01$). Both powders present a high delivered dose (emitted dose), with 89 ± 6% (mean ± SD) for the Hi_Agg_DP and 93 ± 5 % for the Lo_Agg_DP ($p > 0.05$). The majority of the deposition occurred on stages 3 and 4, which accounted for approximately 60% of the delivered dose in the [4.46 to 1.66] µm particle size window (Fig 1c). Furthermore, both dry powders exhibited similar MMADs with values of 2.41 ± 0.26 µm for the Hi_Agg_DP and 2.69 ± 0.01 µm for the Lo_Agg_DP ($p > 0.05$) (Fig 1d). Remarkably, the theoretical aerodynamic diameter (d_{aer}) of each powder was almost identical to its measured MMAD, indicating that the powder particles fully de-agglomerated in individual particles during aerosolization in the NGI.

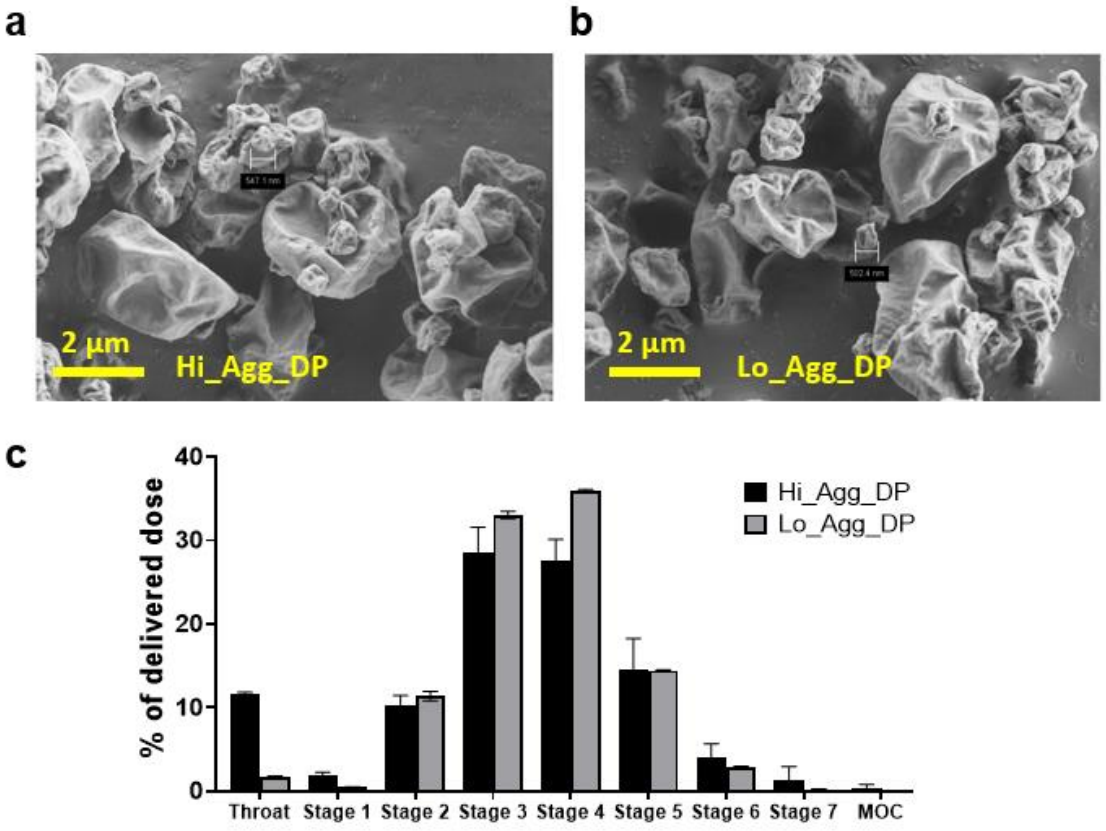

d

	% DD (RSD)	FPF < 5 µm (RSD)	FPF < 3 µm (RSD)	FPF < 1 µm (RSD)	MMAD (RSD)	GSD (RSD)	ρ (SD)	*d* (SD)	d_{aer} (SD)
Hi_Agg_DP	88.5 (6.6)	78.3 (2.1)	51.7 (8.8)	7.3 (56.1)	2.41 (10.65)	1.79 (6.12)	0.42 (0.04)	3.86 (0.49)	2.52 (0.45)
Lo_Agg_DP	92.9 (5.3)	88.6 (0.3)	57.8 (0.0)	4.6 (4.1)	2.69 (0.07)	1.53 (1.03)	0.53 (0.15)	2.96 (0.18)	2.14 (0.31)

Fig 1. Characteristics of rhod-NIP228 dry powder aerosols. Scanning electron microscope (SEM) micrographs of spray dried powders Hi_Agg_DP (**a**) and Lo_Agg_DP (**b**). **c,** data of Next Generation Impactor (NGI) showing the deposition of dry powder particles in each stage as percentage of the delivered dose. Bars represent mean ± SD (n = 2). Cutoffs: stage 1 (8.06 µm), stage 2 (4.46 µm), stage 3 (2.82 µm), stage 4 (1.66 µm), stage 5 (0.94 µm), stage 6 (0.55 µm), and stage 7 (0.34 µm). MOC, miro-orifice collector. **d,** Aerodynamic characteristics of rhod-NIP228 dry powder aerosols. DD, delivered dose; FPF, fine particle fraction (%); GSD, geometric standard deviation; MMAD, mass median aerodynamic diameter; RSD, relative standard deviation; SD, standard deviation; *d*, primary geometric particle diameter; *ρ*, powder density; d_{aer}, primary aerodynamic diameter.

4.2. Protein aggregates characterization

Protein aggregates can be classified into different categories based on their size and, less robustly, on their solubility (Narhi et al., 2012). In this work, protein aggregates that are not removed by centrifugation at 10,000 g for 10 min are invariably referred to as soluble aggregates. They include monomers and oligomers. Aggregates that are eliminated by centrifugation at 10,000 g for 10 min are referred to as insoluble aggregates. They include visible (> 100 µm) and subvisible particles (1–100 µm).

DLS analysis of the solution of rhod-NIP228 showed a monodisperse peak with a hydrodynamic size ca. 10 nm corresponding to monomers of rhod-NIP228 (Fig 2 a). Rhod-NIP228 solution did not contain visible aggregates by confocal microscopy (Fig 2 b) and eluted as a single peak by SEC (Fig 2 c) at the same retention time as the unlabelled NIP228 (Fig 2 k), demonstrating the absence of insoluble and soluble protein aggregates or degradation products. When rhod-NIP228 was spray-dried with or without the addition of 1% PS80 (Lo_Agg_DP and Hi_Agg_DP, respectively), both water-reconstituted dry powders showed the presence of protein aggregates by DLS (Fig 2 d and g); however, significantly higher for Hi_Agg_DP where particles of size 100-1000 nm represented 2.6% (% weight) compared to only 0.7% (% weight) for Lo_Agg_DP. Furthermore, Hi_Agg_DP had 7.1% (% weight) of particles in the micrometres range (> 1 µm) which were not seen for Lo_Agg_DP. DLS is a sensitive method for particle detection. However, since the intensity of the scattered light is proportional to the sixth power of the radius, DLS is biased toward detecting large particles such as protein aggregates (Hawe Andrea, 2020).

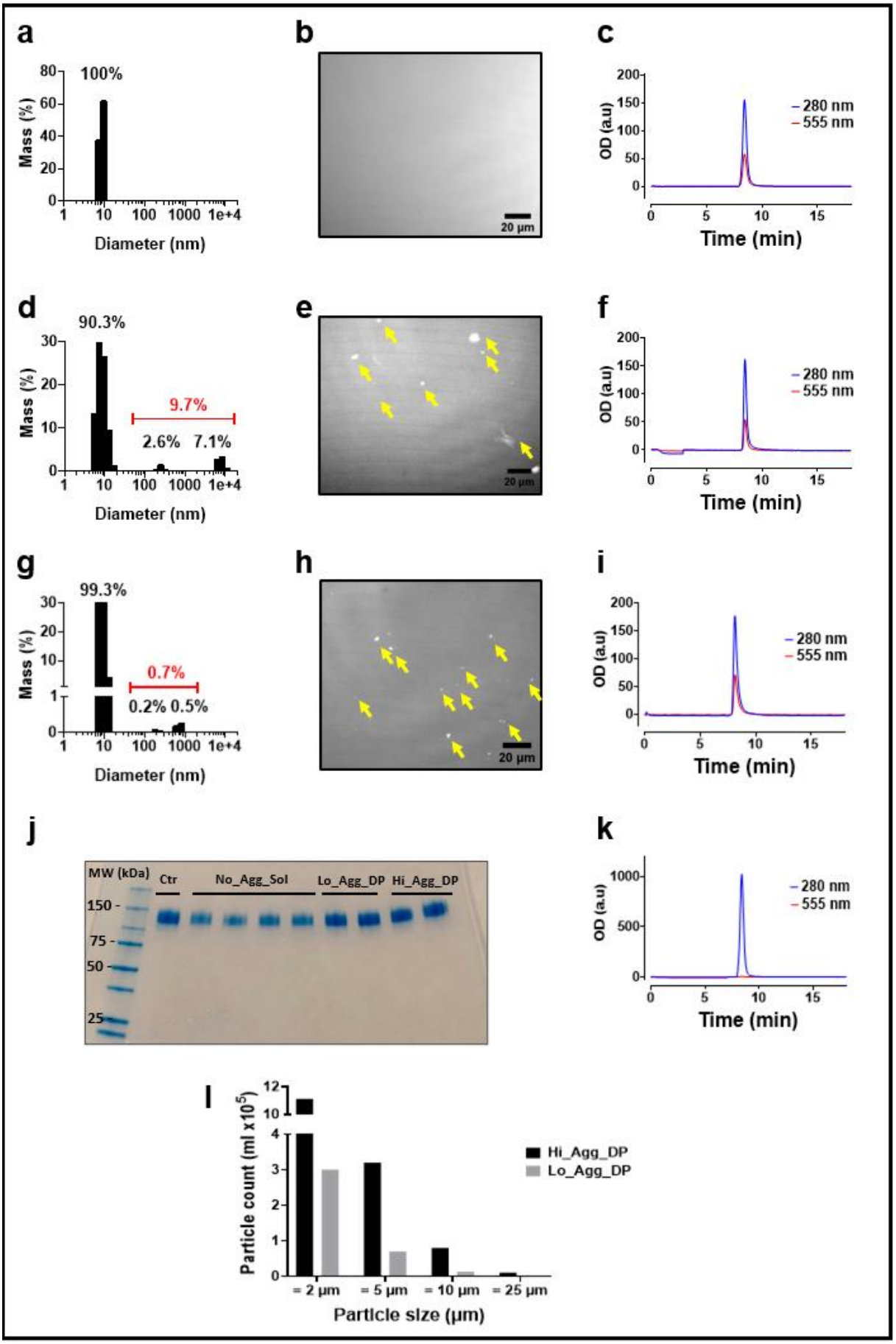
a
100%
Mass (%)
Diameter (nm)
b
20 µm
c
OD (a.u)
280 nm
555 nm
Time (min)
d
90.3%
9.7%
2.6% 7.1%
Mass (%)
Diameter (nm)
e
20 µm
f
OD (a.u)
280 nm
555 nm
Time (min)
g
99.3%
0.7%
0.2% 0.5%
Mass (%)
Diameter (nm)
h
20 µm
i
OD (a.u)
280 nm
555 nm
Time (min)
j
MW (kDa)
Ctr
No_Agg_Sol
Lo_Agg_DP
Hi_Agg_DP
150
75
50
25
k
OD (a.u)
280 nm
555 nm
Time (min)
l
Particle count (ml x10^5)
Hi_Agg_DP
Lo_Agg_DP
= 2 µm
= 5 µm
= 10 µm
= 25 µm
Particle size (µm)

Fig 2. Assessment of protein aggregates of different rhod-NIP228 formulations: rhod-NIP228 solution (= No_Agg_Sol, a-c), reconstituted Hi_Agg_DP (d-f) and reconstituted Lo_Agg_DP (g-i) in distilled water. The hydrodynamic size distributions were measured by dynamic light scattering for rhod-NIP228 solution, Hi_Agg_DP, and Lo_Agg_DP (a, d, and g respectively). Insoluble aggregates were imaged by fluorescence confocal microscopy. Images were acquired using laser line 561 nm and presented in grayscale. Protein aggregates appear as bright spots (yellow arrows) in micrographs corresponding to the reconstituted Hi_Agg_DP (e) and reconstituted Lo_Agg_DP (h) but not the rhod-NIP228 solution (b). c, f, and I, and k, chromatograms of SEC of rhod-NIP228 solution, reconstituted Hi_Agg_DP and reconstituted Lo_Agg_DP, and unlabeled NIP228 after centrifugation at 10,000 g for 10 min. Column was eluted using PBS and peaks were monitored at 280 nm (blue, protein) and 555 nm (red, fluorescent label). j, gel electrophoresis (SDS-PAGE) followed by coomassie blue staining of unlabeled NIP228 (Ctr) and rhod-NIP228 formulations (2-4 µg protein). Molecular weight (MW) ladder on the first lane from the left. k, Micro-flow imaging of water-reconstituted dry powders of Hi_Agg_DP and Lo_Agg_DP at a protein concentration of 5 mg/ml. a.u, arbitrary unit**.**

Confocal images showed the presence of aggregates (> 0.3 µm) in both Hi_Agg_DP and Lo_Agg_DP (Fig 2 e&h); however, no soluble aggregates or degradation products were detected by SEC (Fig 2 f&i). Gel electrophoresis (SDS-PAGE) showed that there are no protein fragments and no covalently formed aggregates (Fig 2 j).

Measuring subvisible particles by microflow imaging confirmed the presence of insoluble aggregates in the micrometer range by measuring particles of size ≥ 2 µm (Fig 2l). Compared with reconstituted Lo_Agg_DP, reconstituted Hi_Agg_DP contained a significantly higher number of particles of sizes of ≥ 2µm (3.7 fold), ≥ 5µm (4.5 fold), ≥ 10µm (6 fold), and ≥ 25µm (8.2 fold); the higher the particle size, the higher the increase in ratio. Moreover, particles of size 2-5 µm were dominant in both reconstituted powders (around two-thirds of all measured particles).

In summary, DLS data indicated the presence of 9.7% insoluble protein aggregates for reconstituted Hi_Agg_DP (by mass), while the reconstituted Lo_Agg_DP showed only 0.7%, and the solution No_Agg_Sol showed none. There were no detectable soluble aggregates in any of the formulations.

4.3. Lung local distribution of rhod-NIP228 solution and dry powders

The local distribution for rhod-NIP228 in lung airspaces and the possibility of *in-situ* protein aggregation in contact with lung surfactant after pulmonary delivery was assessed over time in mice by confocal microscopy.

Immediately after intratracheal instillation of rhod-NIP228 solution, the fluorescence signal was detected in most lung lobes and regions. The signal distribution was somehow homogenous in airspaces but not present in alveolar septa (Fig 3.a). No particular accumulation pattern or, more importantly, aggregates were detected. Note that the resolution of the method is in the range of 0.2 - 0.3 µm, therefore, only aggregates of larger apparent size could be observed. In contrast, both dry powders (Hi_Agg_DP and Lo_Agg_DP) exhibited a rather patchy signal distribution. The fluorescent signal was detected in some regions of the lungs but not in others. The lung distribution of Lo_Agg_DP was only recorded at time 0h and was similar to that of Hi_Agg_DP.

Moreover, images showed the presence of bright spots of larger sizes (Fig 3b, triangles); however, a somewhat more homogenous signal, consistent with dissolved protein, was detected in some regions. Clumps of large sizes (up to 80 µm) were occasionally seen primarily in large upper airways (Fig S4 g). They were attributed to the insufflation procedure where clumps could have formed during the process of loading the dry powders in PE tubing (stacked powder) or due to airways obstruction by the relatively high amounts of dry powder administered to mice by insufflation (~ 0.55 mg). The signal intensity in airspaces decreased after 4h but was still detectable at 16h in all formulations. The fluorescent signal became stronger in AMs (signal was sometimes detected in AMs even at time 0h) and even in lung parenchyma at 4h and 16h. Note that signal from the free dye (Rhodamine) in the lungs drops rapidly to insignificant levels within 4 hours as shown in our previous work (Mahri et al., 2021). It is important to highlight that using a real aerosol inhalation procedure and lower, more clinically relevant doses, were not achievable in this study. These limitations are due to technical challenges associated with the small size of the animals and the difficulty in achieving precise and controlled delivery of small amounts of dry powder using the commercially available insufflators.

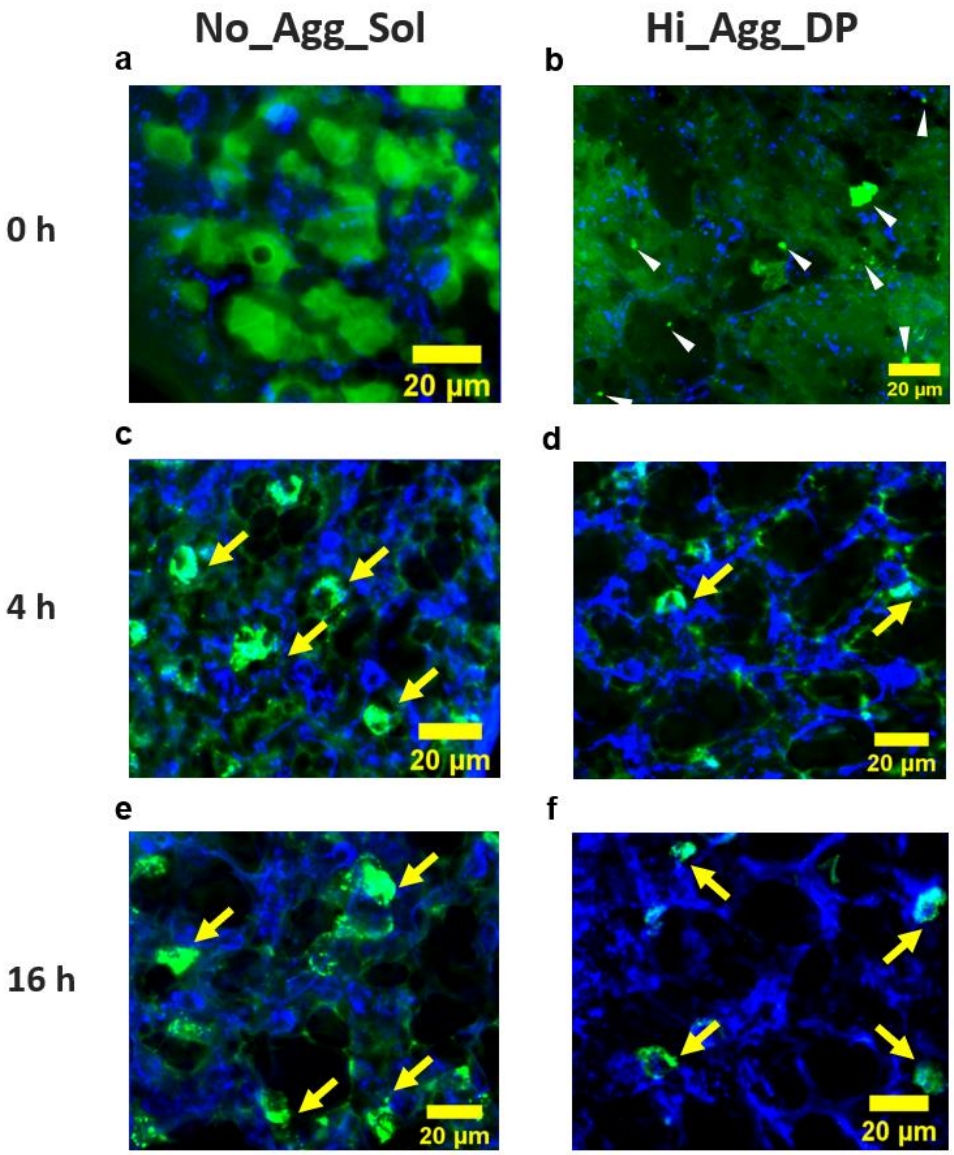

Fig 3. Representative confocal images of the local distribution of rhod-NIP228 formulations in mouse lungs. 50 µg (0.33 nmol) of rhod-NIP228 were administered as a solution by intratracheal instillation (No_Agg_Sol, images a, c, and e) or a powder by intratracheal insufflation (Hi_Agg_DP, images b, d, and f). Mice were sacrificed immediately (a and b), 4h (c and d) or 16h (e and f) post-delivery and the lungs were resected, sliced, then imaged with Cell Observer Spinning Disk (COSD, Zeiss, Germany). Rhod-NIP228 was pseudo-colored in green, and tissue autofluorescence in blue. Each experimental condition was repeated at least twice. Triangles point to bright spots (b); arrows point to AMs (c-f).

4.4. Immunogenicity of rhod-NIP228 solution and dry powders by inhalation and subcutaneous injection

The immunogenicity of rhod-NIP228 solution and dry powder formulations was assessed by pulmonary and subcutaneous delivery in healthy immunocompetent mice. Mice received once a week dose of 50 µg rhod-NIP228 for 4 weeks (5 doses in total) and were sacrificed 18 days after the last dose to determine the levels of IgG ADAs against rhod-NIP228 in sera and BAL (Fig 4a). ADAs titers were also measured in sera at day 20, a day before the 4th administration.

There was no significant difference in the ADA levels measured in sera or BALs 18 days after the last administration among the groups that received rhod-NIP228 by the pulmonary route regardless of the formulation (solution or dry powders). Moreover, all mice of the pulmonary route developed significant levels of anti-NIP228 ADAs (10/10 in each group) compared with weaker responses in the subcutaneous group. A similar trend was observed in BAL (Fig 4c). Transport of antibodies, as well as other proteins, from the serum to the lungs, although poor, is a well-known phenomenon and is likely responsible for the presence of ADAs in BALs (Lombry et al., 2004; Respaud et al., 2015). Furthermore, ADA titers in sera at day 20, one day before the 4th dose, were slightly lower but not significantly different from those in sera at the end of the experiment ($p > 0.7$) (Fig 4d). No significant difference was observed in the body weight among the different groups of mice (Fig 4e), showing a good tolerance to the rhod-NIP228 and the administration procedures (instillation, insufflation, and injection). Only one mouse died during the intratracheal instillation of rhod-NIP228 solution on week 3 during the instillation due to suffocation.

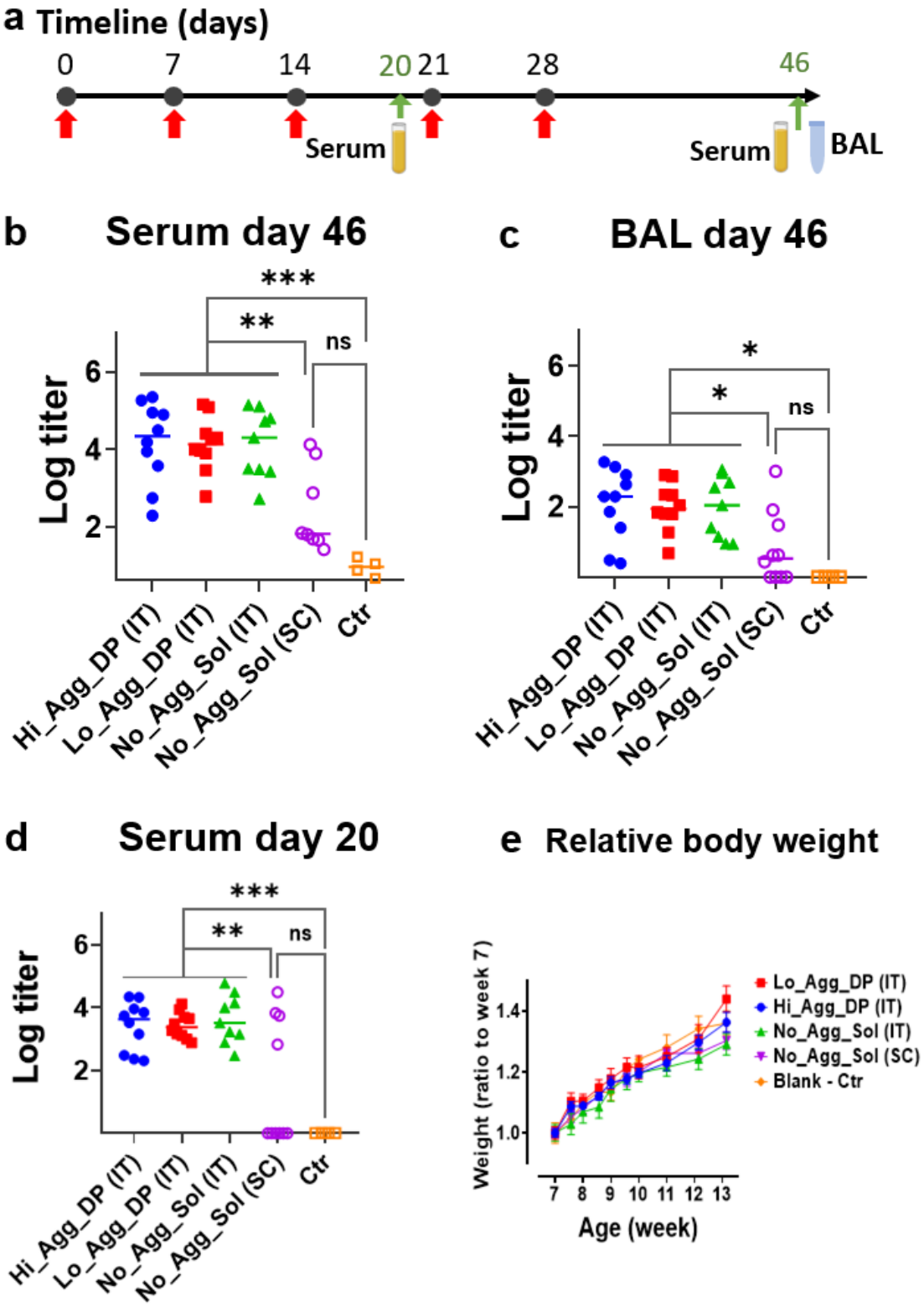

Fig 4. Immunogenicity of different rhod-NIP228 formulations by the pulmonary and subcutaneous routes. **a,** 50 µg (0.33 nmol) of rhod-NIP228 was administered to mice by intratracheal instillation (No_Agg_Sol), intratracheal insufflation of dry powders (Hi_Agg_DP or Lo_Agg_DP), or SC injection of rhod-NIP228 solution (SC). Mice were given 5 once-weekly administrations and were sacrificed 18 days

after the last administration and serum and BAL were collected for ADAs quantification. Control group (Ctr) received a saline solution by intratracheal instillation. ADAs against rhod-NIP228 were detected by ELISA in serum (**b**) and BAL (**c**). **d**, ADA titers in sera at day 20, one day before the fourth dose of rhod-NIP228. **e,** Percentage of weight change normalized to the average weight of each mice group at the beginning of administration on week 7. Note that titers in sera and BALs are not comparable as different thresholds were used. Significant differences are indicated by * $p < 0.05$, ** $p < 0.01$, or *** $p < 0.001$ (b-d, one-way ANOVA on log titers followed with Tukey's post hoc test. e, two-way repeated measures ANOVA followed with Bonferroni post hoc test). ADA, anti-drug antibody.

4.5. Uptake by lung cells

The in vivo uptake of rhod-NIP228 by alveolar macrophages (AMs), interstitial macrophages (IMs), and dendritic cells (DCs) was quantified by flow cytometry 16h following the administration of 50 µg of the different rhod-NIP228 formulations (solution, Hi_Agg_DP, or Lo_Agg_DP) or control (saline). The AM uptake of rhod-NIP228 from the solution was higher than both dry powders, both in terms of fluorescence intensity (3-fold increase, Fig 5a) and percentage of rhodamine positive cells (98% vs 91%, Fig 5b). No statistically significant differences were observed in either fluorescence intensity or the percentage of rhodamine-positive cells between the Hi_Agg_DP and Lo_Agg_DP. Upon excluding rhodamine-negative AMs from the analysis, the fluorescence intensity signal in the solution group remained notably higher, albeit dropping from a 3-fold to 1.6-fold. The fluorescence intensity signal for the Hi_Agg_DP remained non significantly different to the one of the Lo_Agg_DP (Fig S7).

The uptake by IMs and DCs isolated from the lung tissue was very low and statistically not different among rhod-NIP228 groups or compared with the control group (Fig 5c&d). The in vitro uptake of rhod-NIP228 by murine AMs (MHS cell line) was in disagreement with the in vivo data and rather fully correlated with the levels of insoluble aggregates in the formulations, i.e., Hi_Agg_DP > Lo_Agg_DP > Solution (Fig 5f). Puzzled by this contradiction, we evaluated the content of rhod-NIP228 in BAL supernatants at the time of sacrifice (16h) by measuring BAL fluorescence at rhodamine wavelengths (Fig 5e). Results showed that the content of rhod-NIP228 (as a percentage of the administered dose) was significantly higher in BALs of mice that received the solution (49.6 ± 1.1 % [mean ± sem]) compared with those that received either dry powder (31.1 ± 2.0 % for Hi_Agg_DP and 42.0 ± 1.7 % for Lo_Agg_DP).

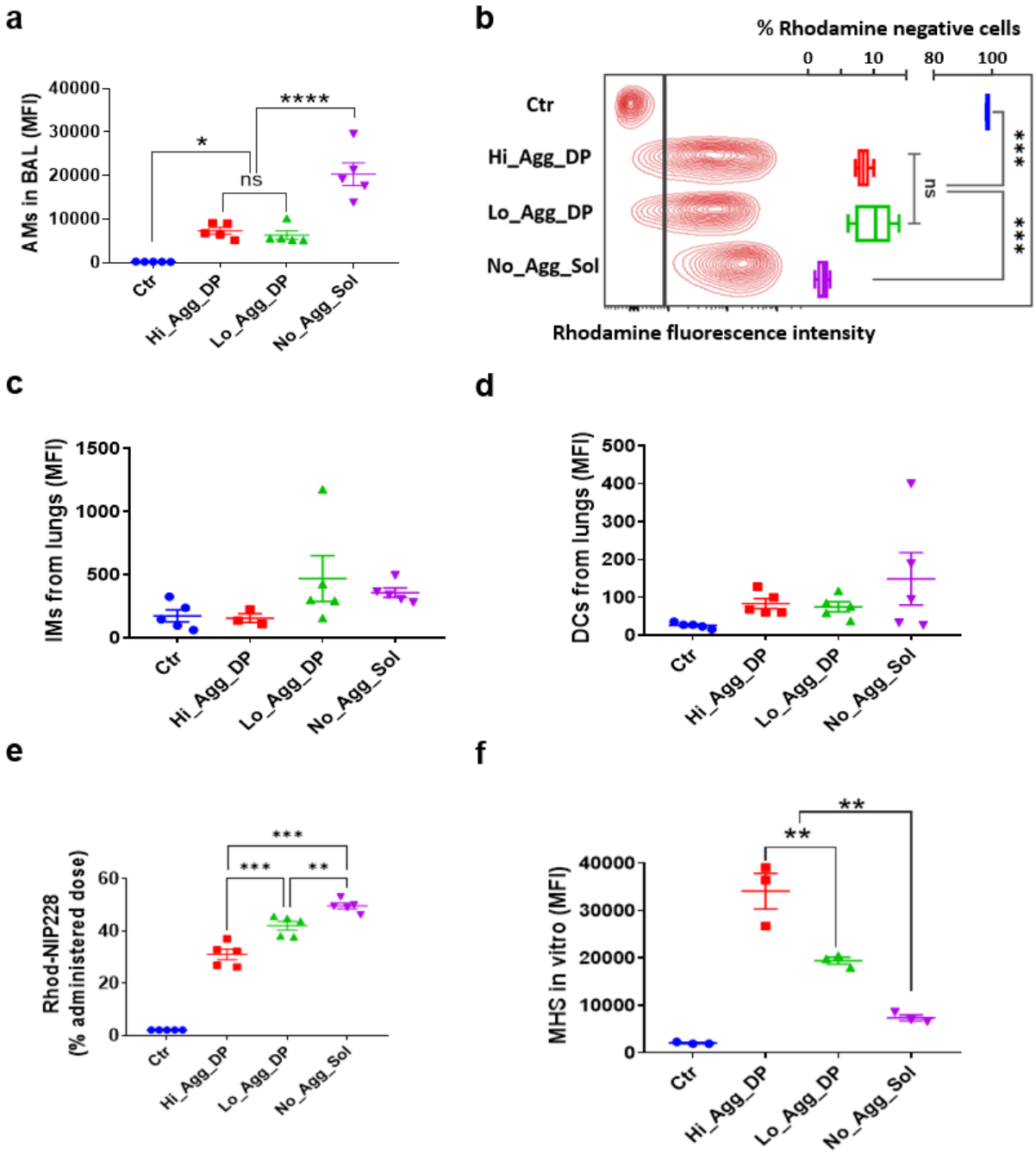

Fig 5. Uptake of rhod-NIP228 by lung cells. **a**, in vivo uptake by alveolar macrophages (AMs) in BAL expressed as median fluorescence intensity (MFI) of all AMs; b**,** percentage of rhodamine negative AMs (right) with representative AMs populations (left). In vivo uptake by interstitial macrophages (IMs, **c**) and dendritic cells (DCs, **d**) in the lungs expressed as median fluorescence intensity (MFI) of all cells. Mice were sacrificed 16h following the delivery of 50 µg (0.33 nmol) of rhod-NIP228 solution (No_Agg_Sol) or dry powders (Hi_Agg_DP or Lo_Agg_DP). The control group (Ctr) received saline by intratracheal instillation. AMs were collected by bronchoalveolar lavage. IMs and DCs were analyzed in the lungs after resection and digestion. The data represent the mean values ± sem (n = 5). **e,** percentage of delivered dose of rhod-NIP228 recovered in mice BALs 16h post administration. Content

of rhod-NIP228 was quantified in the BAL supernatant by spectrofluorometer at 555 nm/600 nm (ex/em). **f**, In vitro uptake by MHS cells. Cells were exposed to 5 µg/ml of rhod-NIP228 for 16 h then cells were harvested and analyzed by flow cytometry. Dry powders were first reconstituted in water then diluted in cell culture medium at target final concentration. Significant differences are indicated by * $p < 0.05$, ** $p < 0.01$, or *** $p < 0.001$ using one-way ANOVA followed with Tukey's post hoc test.

5. Discussion

This study showed that the human mAb NIP228 exhibited higher immunogenicity when administered via the pulmonary route compared to subcutaneous delivery in mice. Interestingly, anti-drug antibodies (ADAs) targeting NIP228 showed consistent levels across different formulations for inhalation, regardless of the presence or absence of protein aggregates.

The first step in this work was to generate dry powders of rhod-NIP228 yielding high and low levels of protein aggregates upon dissolution. Trileucine and trehalose, both known to reduce protein aggregation during spray drying (Lechuga-Ballesteros et al., 2008), did not entirely prevent aggregate formation as relatively high levels of submicron and micron aggregates were still detected after dissolving Hi_Agg_DP (ca. 10%). The incorporation of PS80 surfactant (1% w/w) significantly reduced aggregate formation during spray drying but did not prevent it completely (ca. 0.7% in Lo_Agg_DP). Surfactants reduce protein aggregation during spray drying by interacting with the hydrophobic regions of unfolded proteins and competing for denaturing interfaces like the air-liquid interface (Chang et al., 2021; Eedara et al., 2021; Faghihi, Najafabadi and Vatanara, 2017). PS80 reduced the levels of particulate matter by at least 6-fold for particles ≥ 10 µm and ≥ 25 µm. It is important to highlight that there are currently no regulatory limits for the levels of insoluble particulate matter in inhalation products. However, the guideline outlined in USP Chapter 787 on subvisible particulate matter in therapeutic protein injections can serve as a valuable reference framework for assessing particulate matter in inhaled products. It recommends no more than 3,000 particles ≥ 10 µm and 300 particles ≥ 25 µm by microscopy in low volume parenterals (≤100 mL), which are most relevant to inhaled products (Hickey and Stewart, 2022). According to this guideline, both the Hi_Agg_DP and the Lo_Agg_DP of this study were above these thresholds for a typical 20 mg mAb dose (Burgess et al., 2018). Yet, the USP Chapter 787 recommendation aims to avoid

blood capillary occlusion due to particles rather than immunogenicity and it also does not consider that protein aggregation may occur after administration in situ.

Both dry powders exhibited high fine particle fraction (at least 78 % of FPF < 5 µm) and MMAD ca. 2.5 µm, were prepared with generally recognized as safe excipients and are therefore highly suitable for pulmonary delivery. In fact, particle size of 1–5 µm allows deposition into most pulmonary regions, both bronchial and alveolar (Ibrahim and Garcia-Contreras, 2013). PS80 was found to improve the FPF < 5 µm but did not significantly affect the dry powder's particle morphology and other aerodynamic properties. Trileucine is known to form corrugated particles with reduced cohesiveness and superior aerosol performance than spherical particles with smooth surfaces (Lechuga-Ballesteros et al., 2008). The wrinkled particle shape of the powders is thought to be due to the faster evaporation rate at the droplet surface than the diffusion rate of low solubility and/or large MW components (e.g., trileucine and NIP228) to the center and the ensuing collapse of the crust (Vehring, 2008). Although trehalose and histidine are generally recognized as safe and approved for other routes, they do not appear on the list of inactive ingredients of the FDA as excipients for inhalation (FDA, 2024). A combination of trileucine and trehalose was shown to be tolerated in healthy adults receiving ribavirin by inhalation (Dumont et al., 2020). Moreover, trehalose was well tolerated in 1 to phase 3 trials of Yutrepia (treprostinil) (Roscigno et al., 2020), which was recently granted a tentative FDA approval (August 2024).

The study further investigated the fate of the three rhod-NIP228 formulations in the lungs by confocal microscopy after intratracheal administration in mice. Overall homogeneous distribution of rhod-NIP228 was observed in confocal images of mouse lungs for the instilled solution. In contrast, insufflation of the dry powders resulted in a patchier and heterogeneous distribution and showed the presence of bright spots and large clumps in the lungs. Given the excellent aerodynamic properties of both powders (Table 1), the patchier distribution and the predominant deposition of the powders in the upper airways and trachea are likely due to the powder compaction within the insufflator and the high air velocity during the insufflation manoeuvre (Codrons et al., 2004; Tomar et al., 2019; Tonnis et al., 2014). Airways obstruction by the relatively large amounts of dry powder administered (0.55 mg per mouse or 18 mg per

kg of mouse body weight) might have caused the large clumps while the bright spots might be attributed to protein aggregates from the dry powders.

Despite the presence of different levels of protein aggregates between the dry powders, the immunogenicity of rhod-NIP228 (as measured by ADAs levels) following pulmonary delivery was not affected. This finding lends no support to the prevailing assumption that protein aggregates are inherently more immunogenic than monomers, a notion however primarily based on observations post parenteral administration (Rosenberg, 2006). Secher *et al.* showed that murine IgG aggregates produced during nebulization induced immune cell activation and immunocytotoxicity in vivo in the lungs of C57BL/6 mice following inhalation. Notably, this cytotoxic effect was reduced by improving IgG stability during nebulization (Secher et al., 2022). While some studies reported an increase in immunogenicity of foreign proteins following injection in mice due to the presence of protein aggregates, in other studies, the immunogenicity of the native foreign protein was so high that it overshadowed any additional effect from protein aggregates (Jiskoot et al., 2016). This overshadow might be the case here too. However, it is worth noting that selecting a human antibody in our study was informed by observations from other groups who reported limited or no immunogenicity in mice when murine antibodies were utilized (Kijanka et al., 2018; Secher et al., 2022). Additionally, a key advantage of this study lies in the utilization of protein aggregates derived from a pertinent manufacturing process, as opposed to artificially generated ones.

Literature for other routes of administration suggests that the risk of immunogenicity may increase with aggregate dose, dosing frequency, and possibly particle size (Jiskoot et al., 2016). The effect of aggregate size on immunogenicity is not well-established because of confounding factors in studies. Some publications suggest that submicron aggregates (100-1000 nm) may be more immunogenic (Kijanka et al., 2018) while others suggest that other properties of aggregates such as chemical and physical modifications have a similar or greater impact on immunogenicity than size (e.g, metal-catalyzed oxidized IgG were immunogenic than shaken, pH-shifted or heated formulations) (Filipe et al., 2012; Jiskoot et al., 2016).

AMs appeared to be the main immune cells taking up rhod-NIP228 in the lungs with very little involvement of DCs and IMs, in agreement with previous reports (Vanbever et al., 2019).

Uptake of rhod-NIP228 by macrophages in vitro correlated positively with the aggregate content of the formulations. This observation is consistent with the idea that protein aggregates are more avidly taken up by macrophages than proteins in solution as a result of particles phagocytosis. The trend was opposite in vivo and we rationalize this observation by the higher local availability and deeper and more homogeneous penetration of rhod-NIP228 solution into the lungs following intratracheal instillation, as was confirmed by confocal imaging, flow cytometry and fluorescence quantification in BALs. Differential uptake of rhod-NIP228 from the three formulations by DCs or IMs was not evident due to the weak signal, even though a tendency of higher uptake by DCs was observed for the solution. AMs are poor antigen-presenting cells (Hussell and Bell, 2014), and they might thus prevent the generation of unwanted ADA due to protein aggregates because they quickly eliminate them by phagocytosis.

Having lower incidence of ADAs by SC injection compared with intratracheal instillation indicates that the pulmonary route could be more immunogenic than the subcutaneous route. Recent data from preclinical toxicology studies of inhaled biotherapeutics support this view with a clear trend of increasing ADA incidence in studies of longer duration (Hall et al., 2021). Consistent with our findings, a 3-months case study in NHP (non-human primates) found that an undisclosed tested peptide/protein caused a higher incidence of serum ADA by inhalation compared with a minimal incidence in the subcutaneous group (Hall et al., 2021). Likewise, available clinical data showed that the inhalation route was more immunogenic than the parenteral route for insulin (Exubera, dry powder), acknowledging however that the inhaled dose was also higher than the subcutaneous dose (Skyler et al., 2008). Recombinant human deoxyribonuclease (Pulmozyme®), the only protein administered by nebulization used to treat cystic fibrosis, is very well tolerated in pediatric patients with less than 5% of ADAs in clinical trials (1993). Despite seeing ADAs, the above-mentioned treatments were well-tolerated, and no adverse clinical consequences resulted from ADAs. Neutralising antibodies to ALX-0171 (a trivalent nanobody directed towards the respiratory syncytial virus fusion protein) were detected at day 14 in 30% of the children daily treated with nebulized ALX-0171 from day 1 to day 3, compared with 5% of the children in the placebo group (Cunningham et al., 2021). However, no clear link appeared between neutralising antibody response and time for the

viral load to drop among the different dose study groups and no effect of these antibodies on serum ALX-0171 concentrations were observed.

Whilst acknowledging the challenges of translating preclinical immunogenicity into patient immunogenicity, the present study confirms that the inhalation route may be associated with increased risk for immunogenicity compared to subcutaneous dosing, which needs case-by-case risk-benefit assessment. Our study does not however lend any support to the notion that protein aggregates are important drivers for immunogenicity following pulmonary delivery. Additional preclinical studies using real aerosol inhalation procedure at lower, clinically relevant, doses are now required to first study the presence of protein aggregates in the lungs following dry powder inhalation and determine the categories of these aggregates and second to investigate to which extent such aggregates would add on top of the immunogenicity from the protein itself. These factors are important considerations in the pharmaceutical development of inhaled biologics.

6. Acknowledgements

The authors would like to thank Nicolas Dauguet the responsible of the Flow Cytometry and Cell Sorting Facility at de Duve Institute (UCLouvain, Brussels) for kindly helping in the selection of markers and the setup of the flow cytometry, Steven Oag for his help with the insufflator, and Nick Bond for the provision of NIP228. This work was funded by a research grant from AstraZeneca. Sohaib Mahri received a complementary COVID-19 postdoctoral researcher funding from UCLouvain. Rita Vanbever is Research Director of the Fonds National de la Recherche Scientifique (FNRS, Belgium). Donatienne Tyteca and François Huaux are both Senior Research Associate of the FNRS.

7. References

1993. Pulmozyme. Product monograph.
Burgess, G., Boyce, M., Jones, M., Larsson, L., Main, M.J., Morgan, F., Phillips, P., Scrimgeour, A., Strimenopoulou, F., Vajjah, P., Zamacona, M., Palframan, R., 2018. Randomized study of the safety and pharmacodynamics of inhaled interleukin-13 monoclonal antibody fragment VR942. EBioMedicine 35, 67-75.
Chang, R.Y.K., Chow, M.Y.T., Khanal, D., Chen, D., Chan, H.K., 2021. Dry powder pharmaceutical biologics for inhalation therapy. Adv Drug Deliv Rev 172, 64-79.
Codrons, V., Vanderbist, F., Ucakar, B., Preat, V., Vanbever, R., 2004. Impact of formulation and methods of pulmonary delivery on absorption of parathyroid hormone (1-34) from rat lungs. J Pharm Sci 93, 1241-1252.
Cunningham, S., Piedra, P.A., Martinon-Torres, F., Szymanski, H., Brackeva, B., Dombrecht, E., Detalle, L., Fleurinck, C., group, R.s., 2021. Nebulised ALX-0171 for respiratory syncytial virus lower respiratory tract infection in hospitalised children: a double-blind, randomised, placebo-controlled, phase 2b trial. Lancet Respir Med 9, 21-32.
Desoubeaux, G., Reichert, J.M., Sleeman, M., Reckamp, K.L., Ryffel, B., Adamczewski, J.P., Sweeney, T.D., Vanbever, R., Diot, P., Owen, C.A., Page, C., Lerondel, S., Le Pape, A., Heuze-Vourc'h, N., 2016. Therapeutic monoclonal antibodies for respiratory diseases: Current challenges and perspectives, March 31 - April 1, 2016, Tours, France. MAbs 8, 999-1009.
Dumont, E.F., Oliver, A.J., Ioannou, C., Billiard, J., Dennison, J., van den Berg, F., Yang, S., Chandrasekaran, V., Young, G.C., Lahiry, A., Starbuck, D.C., Harrell, A.W., Georgiou, A., Hopchet, N., Gillies, A., Baker, S.J., 2020. A Novel Inhaled Dry-Powder Formulation of Ribavirin Allows for Efficient Lung Delivery in Healthy Participants and Those with Chronic Obstructive Pulmonary Disease in a Phase 1 Study. Antimicrob Agents Chemother 64.
Eedara, B.B., Alabsi, W., Encinas-Basurto, D., Polt, R., Mansour, H.M., 2021. Spray-Dried Inhalable Powder Formulations of Therapeutic Proteins and Peptides. AAPS PharmSciTech 22, 185.
Faghihi, H., Najafabadi, A.R., Vatanara, A., 2017. Optimization and characterization of spray-dried IgG formulations: a design of experiment approach. Daru 25, 22.
FDA, 2014. Guidance for Industry: Immunogenicity Assessment for Therapeutic Protein Products.
FDA, 2024. https://www.accessdata.fda.gov/scripts/cder/iig/index.cfm.
Filipe, V., Jiskoot, W., Basmeleh, A.H., Halim, A., Schellekens, H., Brinks, V., 2012. Immunogenicity of different stressed IgG monoclonal antibody formulations in immune tolerant transgenic mice. MAbs 4, 740-752.
Hall, A.P., Tepper, J.S., Boyle, M.H., Cary, M.G., Flandre, T.G., Piaia, A., Tarnow, I., Macri, N.P., Freke, M.C., Nikula, K.J., Paul, G.R., Cauvin, A., Gregori, M., Haworth, R., Naylor, S., Price, M., Robinson, I.N., Allen, A., Gelzleichter, T., Hohlbaum, A.M., Manetz, S., Wolfreys, A., Colman, K., Fleurance, R., Jones, D., Mukaratirwa, S., 2021. BSTP Review of 12 Case Studies Discussing the Challenges, Pathology, Immunogenicity, and Mechanisms of Inhaled Biologics. Toxicol Pathol 49, 235-260.
Hawe Andrea, W.D., Zölls Sarah, Reichel Angelika, Carpenter John F. , 2020. Submicrometer, micrometer and visible particle analysis in biopharmaceutical research and development, in: Damian J. Houde, S.A.B. (Ed.), Biophysical Characterization of Proteins in Developing Biopharmaceuticals, Second ed. Elsevier, pp. 285-310.
Hickey, A.J., Stewart, I.E., 2022. Inhaled antibodies: Quality and performance considerations. Hum Vaccin Immunother 18, 1940650.
Hussell, T., Bell, T.J., 2014. Alveolar macrophages: plasticity in a tissue-specific context. Nat Rev Immunol 14, 81-93.
Ibrahim, M., Garcia-Contreras, L., 2013. Mechanisms of absorption and elimination of drugs administered by inhalation. Ther Deliv 4, 1027-1045.

Ibrahim, M., Wallace, I., Ghazvini, S., Manetz, S., Cordoba-Rodriguez, R., Patel, S.M., 2023. Protein Aggregates in Inhaled Biologics: Challenges and Considerations. J Pharm Sci 112, 1341-1344.
Jiskoot, W., Kijanka, G., Randolph, T.W., Carpenter, J.F., Koulov, A.V., Mahler, H.C., Joubert, M.K., Jawa, V., Narhi, L.O., 2016. Mouse Models for Assessing Protein Immunogenicity: Lessons and Challenges. J Pharm Sci 105, 1567-1575.
Kijanka, G., Bee, J.S., Korman, S.A., Wu, Y., Roskos, L.K., Schenerman, M.A., Slutter, B., Jiskoot, W., 2018. Submicron Size Particles of a Murine Monoclonal Antibody Are More Immunogenic Than Soluble Oligomers or Micron Size Particles Upon Subcutaneous Administration in Mice. J Pharm Sci 107, 2847-2859.
Labiris, N.R., Dolovich, M.B., 2003. Pulmonary drug delivery. Part II: the role of inhalant delivery devices and drug formulations in therapeutic effectiveness of aerosolized medications. Br J Clin Pharmacol 56, 600-612.
Lechuga-Ballesteros, D., Charan, C., Stults, C.L., Stevenson, C.L., Miller, D.P., Vehring, R., Tep, V., Kuo, M.C., 2008. Trileucine improves aerosol performance and stability of spray-dried powders for inhalation. J Pharm Sci 97, 287-302.
Lombry, C., Marteleur, A., Arras, M., Lison, D., Louahed, J., Renauld, J.C., Preat, V., Vanbever, R., 2004. Local and systemic immune responses to intratracheal instillation of antigen and DNA vaccines in mice. Pharm Res 21, 127-135.
Mahri, S., Rondon, A., Wilms, T., Bosquillon, C., Vanbever, R., 2021. Biodistribution and elimination pathways of PEGylated recombinant human deoxyribonuclease I after pulmonary delivery in mice. J Control Release 329, 1054-1065.
Narhi, L.O., Schmit, J., Bechtold-Peters, K., Sharma, D., 2012. Classification of protein aggregates. J Pharm Sci 101, 493-498.
Osman, N., Kaneko, K., Carini, V., Saleem, I., 2018. Carriers for the targeted delivery of aerosolized macromolecules for pulmonary pathologies. Expert Opin Drug Deliv 15, 821-834.
Respaud, R., Vecellio, L., Diot, P., Heuze-Vourc'h, N., 2015. Nebulization as a delivery method for mAbs in respiratory diseases. Expert Opin Drug Deliv 12, 1027-1039.
Roscigno, R., Vaughn, T., Anderson, S., Wargin, W., Hunt, T., Hill, N.S., 2020. Pharmacokinetics and tolerability of LIQ861, a novel dry-powder formulation of treprostinil. Pulm Circ 10, 2045894020971509.
Rosenberg, A.S., 2006. Effects of protein aggregates: an immunologic perspective. AAPS J 8, E501-507.
Secher, T., Bodier-Montagutelli, E., Parent, C., Bouvart, L., Cortes, M., Ferreira, M., MacLoughlin, R., Ilango, G., Schmid, O., Respaud, R., Heuze-Vourc'h, N., 2022. Aggregates Associated with Instability of Antibodies during Aerosolization Induce Adverse Immunological Effects. Pharmaceutics 14.
Shankar, G., Arkin, S., Devanarayan, V., Kromminga, A., Quarmby, V., Richards, S., Subramanyam, M., Swanson, S., 2015. The quintessence of immunogenicity reporting for biotherapeutics. Nat Biotechnol 33, 334-336.
Skyler, J.S., Hollander, P.A., Jovanovic, L., Klioze, S., Krasner, A., Riese, R.J., Reis, J., Schwartz, P., Duggan, W., Inhaled Human Insulin Type 1 Diabetes Study, G., 2008. Safety and efficacy of inhaled human insulin (Exubera) during discontinuation and readministration of therapy in adults with type 1 diabetes: A 3-year randomized controlled trial. Diabetes Res Clin Pract 82, 238-246.
Tao, Y., Chen, Y., Howard, W., Ibrahim, M., Patel, S.M., McMahon, W.P., Kim, Y.J., Delmar, J.A., Davis, D., 2023. Mechanism of Insoluble Aggregate Formation in a Reconstituted Solution of Spray-Dried Protein Powder. Pharm Res 40, 2355-2370.
Tomar, J., Tonnis, W.F., Patil, H.P., de Boer, A.H., Hagedoorn, P., Vanbever, R., Frijlink, H.W., Hinrichs, W.L.J., 2019. Pulmonary immunization: deposition site is of minor relevance for influenza vaccination but deep lung deposition is crucial for hepatitis B vaccination. Acta Pharm Sin B 9, 1231-1240.
Tonnis, W.F., Bagerman, M., Weij, M., Sjollema, J., Frijlink, H.W., Hinrichs, W.L., de Boer, A.H., 2014. A novel aerosol generator for homogenous distribution of powder over the lungs after pulmonary administration to small laboratory animals. Eur J Pharm Biopharm 88, 1056-1063.

Vanbever, R., Loira-Pastoriza, C., Dauguet, N., Herin, C., Ibouraadaten, S., Vanvarenberg, K., Ucakar, B., Tyteca, D., Huaux, F., 2019. Cationic Nanoliposomes Are Efficiently Taken up by Alveolar Macrophages but Have Little Access to Dendritic Cells and Interstitial Macrophages in the Normal and CpG-Stimulated Lungs. Mol Pharm 16, 2048-2059.
Vanbever, R., Mintzes, J.D., Wang, J., Nice, J., Chen, D., Batycky, R., Langer, R., Edwards, D.A., 1999. Formulation and physical characterization of large porous particles for inhalation. Pharm Res 16, 1735-1742.
Vehring, R., 2008. Pharmaceutical particle engineering via spray drying. Pharm Res 25, 999-1022.
Walsh, G., 2018. Biopharmaceutical benchmarks 2018. Nat Biotechnol 36, 1136-1145.